**THE EUROPEAN
PHYSICAL JOURNAL PLUS**

Numerical investigation of coalescence phenomena, affected by surface acoustic waves

Arash Shams Taleghani[1,a] , **Mahdi Sheikholeslam Noori**[2]

[1] Aerospace Research Institute, Ministry of Science, Research and Technology, Tehran, Iran
[2] Department of Aerospace Engineering, K. N. Toosi University of Technology, Tehran, Iran

Abstract We investigate numerically the coalescence dynamics of two same droplets on a wettable substrate when the droplets are subjected by the surface acoustic waves (SAW). For this purpose, dynamics of the flow is simulated using Lattice Boltzmann method. At first, the coalescence phenomena are studied. Then, the effects of SAW on behaviors of droplets are illustrated. The results show that in the pumping mode, regardless of the location, the droplets coalesce when the SAWs are applied. Also, we can reduce the connection time about 60% by increasing the wave amplitude. Based on the results, the coalescence time is minimized to a certain wave amplitude that in our study occurs in the wave amplitude number (A_{SAW}) about 16. In the jetting mode, three different dynamical behaviors are observed and are categorized with wave amplitude number. When $A_{SAW} < 8$, the coalescence of two droplets and the detachment of the formed droplet occurs, while we observe the periodic detachment and connection of droplets for $8 < A_{SAW} < 10$. Then, two droplets affected by SAWs are removed from the surface for $A_{SAW} > 10$. Also, we show that $A_{SAW} \approx 14$ is the optimum situation for removal of the droplets from the surface.

1 Introduction

Interfacial phenomena have long occupied the human mind, but we can say that the oldest scientific research on them has been conducted by Young and Laplace [1]. Despite its widespread applications and simple appearance, this phenomenon is very complex and still has many ambiguities. Therefore, the study of these phenomena remains an interesting field of research.

An important and interesting subject in the interfacial phenomena is the problem of coalescence. Yarin [2] has presented a complete review paper about the drop impact dynamics, in which the splashing, spreading, and coalescence phenomena have been investigated from a theoretical, experimental, and numerical point of view. Also, the kinematics and dynamics of the spreading, pinching, and coalescence of droplets were experimentally studied by Fardin et al. in Ref. [3]. Based on scaling law and Ohnesorge number, they extracted three self-similar situations for Newtonian fluids: visco-inertial, visco-capillary, and inertia-capillary. Sui et al. [4] investigated the coalescence of two droplets located on a substrate in partially wetting phenomena. They show that for a 90° contact angle, the height of the connection bridge, with respect to the time, followed a power law with a 2/3 exponent up to a threshold time and beyond that time with a 1/2 exponent. Furthermore, the coalescence of two same droplets on a hydrophilic substrate was experimentally studied in Ref. [5]. The dynamics of coalescence of two spreading droplets has been experimentally and theoretically investigated and the variation of connecting bridge with respect to time has been extracted by Ristenpart et al. [6]. In addition, Erkan investigated the coalescence phenomena for two droplets with different sizes [7], based on Reynolds equation and lubrication assumption. Moreover, the coalescence of two pendant droplets was simulated via molecular dynamics by Liu et al. [8] in the shear gas flow, and the regime diagrams were established.

As an example of applications of coalescence phenomena, separation of water droplets from crude oil was presented by Sian et al. [9]. In this experimental work, a microfluidic device was designed to select the most suitable demulsifier. Coalescence phenomena in emulsion generation are affected by fluids properties, system conditions, and diffusion and adsorption behaviors. A useful device for designing these processes is microfluidic technology. Reference [10] presents a comprehensive review of these devices. Effects of ultrasound phenomena on the water-in-oil emulsion were investigated by Adeyemi et al. [11]. The results of this study showed that using ultrasonic waves, the coalescence time was reduced. Coalescence-induced droplet jumping without requiring any external energy is studied in Ref. [12, 13]. When two droplets coalesce on a superhydrophobic surface, the formed droplet jumps spontaneously. Also, Miot et al. [14] investigated numerical simulation of coalescence of three droplets. Their study was based on an energy method.

Control of the phenomena in the above-mentioned applications is an important issue and so, many researches are conducted in this field. For example, Feng et al. [15] reviewed the passive and active methods of control in the laboratory on a chip. In the field of active control of the coalescence phenomena, we can mention Ref. [16], wherein the coalescence of droplets under AC and DC electric fields was studied. As another method, we can refer to acoustophoresis methods which are presented in Ref. [17].

Acoustofluidics is a modern research field in which fluids and particles are manipulated with acoustic waves that are generated using piezoelectric transducers of typical frequency between a few kHz to several tens of MHz [18]. Di Sun et al. [19] presented a piezoelectric transducer for droplet delivery and nebulization for mass spectrometry. Also, surface acoustic waves were used for droplet generation in Ref. [20]. Biroun et al. [21] developed a numerical model to simulate the interactions between liquid and waves and deformations of fluid–fluid interface. Also, the effect of the location of transducer on droplet dynamics was investigated. Water droplet motion affected by SAWs has been simulated using COMSOL Multiphysics, and the effects of actuation parameters are presented by Insepov et al. [22]. Nozzles jetting, which is very important and crucial in printing, is presented in [23, 24], and droplet jetting at controlled angles was achieved. Brunet and Baudoin [25] investigated the unstationary dynamics of droplets affected by SAW, and the effects of pressure radiation and acoustic streaming were clearly presented.

Another application of SAW and acoustofluidics is manipulation, collection, and separation of micro- and nanoparticles. Based on mechanical properties and size, SAWs can affect the particles. Ozer and Cetin [26] studied the effect of geometry and acoustic properties of chip materials in particle manipulation via ultrasonic waves. A device was proposed in Ref. [27] which used three modes of ultrasonic standing waves to separate particles in different parts of a microchannel.

During the last decade, acoustic manipulation to control special cellular organization has arisen and is used in tissue engineering and regenerative medicine [28]. Also, Liu et al. [29] developed a chip for time-controlled reactions. Furthermore, minimizing droplet impact contact time was investigated by Biroun et al. [30]. Moreover, active mixing of fluids and colloids at nanoscale (that surface and viscous forces are dominant) is experimentally illustrated in Ref. [31]. In addition, a micro-heater using SAW was used in a micro-reactor for temperature control [32]. Further, Lei et al. [33] presented a novel SAW-microfluidic jetting system with a vertical capillary tube, and they showed that this system had apparent advantages in controllable jetting. Application of SAW in sensors was reviewed by Mandal and Banerjee [34]. Also, materials, design, and coating technologies for surface acoustic waves sensors are presented in Ref. [35].

Thermal distribution during SAW liquid atomization was experimentally investigated by Huang et al. [36]. They found that liquid heating was due to viscous dissipation of irradiated wave energy. Also, researches show that droplets affected by intense surface acoustic waves were vaporized if they match the theoretical resonance size [37]. Moreover, a three-layer substrate is presented in Ref. [38], and based on it, a disposable device via SAW was developed. Huang et al. [39] showed that streaming did not significantly affect the temperature in the liquid.

The main goal of this paper is to investigate the coalescence phenomena affected by SAWs. This problem can be applicable in biochemical researches, particle sampling, particle/cell manipulation, removal of water droplets from the surfaces, and collection of droplets from the surfaces. The investigation of the effects of SAW on the dynamics of coalescence such as coalescence time and the hydrodynamics of the final phases of coalescence is the main scope of the present study. Also, the possible morphologies of the entire coalescence of the sessile droplets affected by SAW are explored. For this purpose, a modified color gradient model, based on multi-relaxation time (MRT), was used. The accuracy, stability, and verification of the numerical model is analyzed in Ref. [40]. First, the coalescence of two same droplets located on a substrate is presented in this paper. In this problem, the main novelties of this work comprise of simulation of phenomena using LBM method and the study of physics on hydrophobic surfaces. Also, the obtained results are compared with reliable numerical results and experimental data. Then, the effects of SAWs on the physical behaviors of droplets are illustrated. We studied the modeling of SAWs in our previous works such as [41–43], and the important difference between this work and them is the investigation of the phenomena when two same droplets are subjected by SAWs. Based on our knowledge, this physics has not been previously presented, neither numerically nor experimentally, and this is the most important innovation of this work.

The rest of the present paper is organized as follows: In Sect. 2, the governing equations and the numerical methods are described. Also, a definition of the problem is presented in this section. For validation purposes, numerical results are compared with reliable experimental data. Then, the simulation of acoustofluidics is investigated in the last section of the paper, and it is described both qualitatively and quantitatively. Finally, this manuscript tries to answer the coalescence phenomena how can be controlled, using SAW. How can we reduce the connection time? And, what are the effects of SAW on the formed droplets?

2 Numerical method

In this study, some fluid and flow quantities are calculated using two-phase LBM simulations. Therefore, we applied a color gradient model which was thoroughly described in our previous works [40–43]. So, in order to avoid repetition and prolongation, a brief description of the method is presented here and interested readers should refer to the mentioned works.

The present model has four steps, namely multi-relaxation-time (MRT) single-phase collision, perturbation, streaming, and recoloring step. The streaming step is as follows:

$$f_i^k(\vec{x} + \vec{c}_i \delta t, t + \delta t) = f_i^k(\vec{x}, t) + \left(\Omega_i^k\right)^1 \left(f_i^k(\vec{x}, t)\right) + \left(\Omega_i^k\right)^2 \left(f_i^k(\vec{x}, t)\right). \tag{1}$$

where $f_i^k(\vec{x}, t)$ is the total distribution function in ith velocity direction at position $\vec{x}$ and time t, subscript i is the lattice velocity direction, superscript k represents the red and blue fluids (liquid or gas phases), $\vec{c}_i$ is the lattice velocity in ith direction, and δt is the time step.

The particle velocity vector in a D2Q9 LBM (two dimensions and nine moments) is as follows:

$$\vec{c}_0 = (0, 0), \vec{c}_1 = (1, 0), \vec{c}_2 = (0, 1), \vec{c}_3 = (-1, 0), \vec{c}_4 = (0, -1), \vec{c}_5 = (1, 1), \vec{c}_6 = (-1, 1), \vec{c}_7 = (-1, -1), \vec{c}_8 = (1, -1). \tag{2}$$

Also, $\left(\Omega_i^k\right)^1$ and $\left(\Omega_i^k\right)^2$ are MRT single-phase collision and perturbation operators, respectively. MRT operator is presented in Eqs. (3).

$$\left(\Omega_i^k\right)^1 = -\left(M^{-1}S\right)\left(m_i^k - m_i^{keq}\right) \tag{3}$$

M and its inverse matrix are presented in the appendix. Also, S is a diagonal matrix given by:

$$S = \text{diag}(s_0, s_1, s_2, s_3, s_4, s_5, s_6, s_7, s_8) = \text{diag}(0, s_e, s_\zeta, 0, s_q, 0, s_q, s_v, s_v) \tag{4}$$

where the element s_i represents the relaxation parameter. These parameters are chosen as $s_e = 1.25$, $s_\zeta = 1.14$, $s_q = 1.6$ and, s_v is related to the dynamic viscosity of two fluids and is $\frac{1}{\tau}$ where τ is the relaxation time parameter which is related to fluid viscosity.

The equilibrium distribution function in the interaction mode space, m_i^{keq}, is obtained by:

$$m^{keq} = \rho^k \left(1, -3.6\alpha^k - 0.4 + 3|\vec{u}|^2, 5.4\alpha^k - 1.4 - 3|\vec{u}|^2, u_x, \left(-1.8\alpha^k - 0.2\right)u_x, u_y, \left(-1.8\alpha^k - 0.2\right)u_y, u_x^2 - u_y^2, u_x u_y\right)^T, \tag{5}$$

where $\vec{u}$ is the flow velocity (u_x and u_y are x and y components, respectively), and it is obtained by:

$$\vec{u} = \sum \sum f_i^k \vec{c}_i. \tag{6}$$

α^k is a free parameter that the stable interface assumption requires to satisfy the following relation:

$$\frac{\rho^{R0}}{\rho^{B0}} = \frac{1 - \alpha^B}{1 - \alpha^R} \tag{7}$$

Constraint of $0 \leq \alpha^k \leq 1$ should be satisfied to avoid the unreal value of the speed of sound and the negative value of fluid density. Also, we can write $m_i^k = \sum_j M_{ij} f_j^k$.

Perturbation, $\left(\Omega_i^k\right)^2$ operator is as follows:

$$\left(\Omega_i^k\right)^2 = \frac{A^k}{2} |\vec{f}| \left[w_i \frac{\left(\vec{c}_i \cdot \vec{f}\right)^2}{|\vec{f}|^2} - B_i \right] \tag{8}$$

where A^k is a parameter that affects the interfacial tension and $\vec{f}$ is the color gradient which is calculated as:

$$\vec{f}(\vec{x}, t) = \sum \vec{c}_i \left[\rho^R(\vec{x} + \vec{c}_i \Delta t, t) - \rho^B(\vec{x} + \vec{c}_i \Delta t, t)\right]. \tag{9}$$

Besides, $B_0 = -\frac{4}{27}$, $B_i = \frac{2}{27}$, for $i = 1, 2, 3, 4$ and $B_i = \frac{5}{108}$, for $i = 5, 6, 7, 8$. Using these parameters, the correct term due to interfacial tension in the Navier–Stokes equations can be recovered. Weighted constants w_i are calculated as: $w_0 = \frac{4}{9}$, $w_1 = w_2 = w_3 = w_4 = \frac{1}{9}$, $w_5 = w_6 = w_7 = w_8 = \frac{1}{36}$.
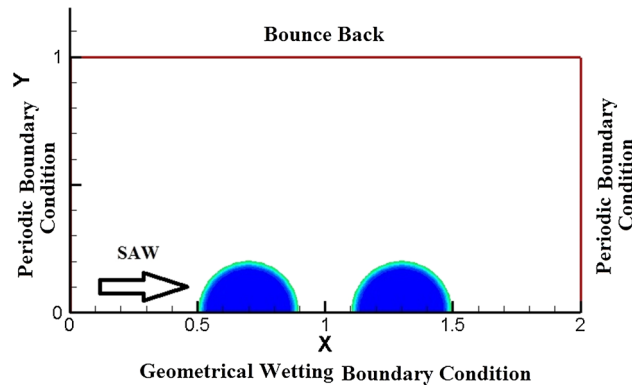
The following equation shows the relationship between surface tension coefficient σ and the parameter A^k:

$$\sigma = \frac{5\rho\left(A^R + A^B\right)}{6\tau}. \tag{10}$$

Recoloring step is presented in Eq. (11):

$$f_i^R(\vec{x}, t) = \frac{\rho^R}{\rho^R + \rho^B}\left(f_i^{\prime R}(\vec{x}, t) + f_i^{\prime B}(\vec{x}, t)\right) + \beta \frac{\rho^R \rho^B}{\rho^R + \rho^B} w_i \cos\varphi_i |\vec{c}_i|, \tag{11-a}$$

$$f_i^B(\vec{x}, t) = \frac{\rho^B}{\rho^R + \rho^B}\left(f_i^{\prime R}(\vec{x}, t) + f_i^{\prime B}(\vec{x}, t)\right) - \beta \frac{\rho^R \rho^B}{\rho^R + \rho^B} w_i \cos\varphi_i |\vec{c}_i|. \tag{11-b}$$

Fig. 1 Physical model

Moreover, $f_i'^k$ is the post-perturbation value of the distribution function, φ_i is the angle between $\vec{\nabla}\rho^N$ and the lattice direction c_i, β is a parameter associated with the interface thickness and should take a value between zero and unity. Phase field, ρ^N, is defined as follows:

$$\rho^N = \left(\frac{\rho^R}{\rho^{R^0}} - \frac{\rho^B}{\rho^{B^0}} \right) \bigg/ \left(\frac{\rho^R}{\rho^{R^0}} + \frac{\rho^B}{\rho^{B^0}} \right), \tag{12}$$

where ρ^{R^0} and ρ^{B^0} are the densities of the pure red and blue fluids, ρ^k is the density of each fluid:

$$\rho^k = \sum_i f_i^k. \tag{13}$$

In this paper, displacement of a two-dimensional drop affected by SAW is studied. The SAW has been modeled using a body force acting on the fluid volume. The procedure of modeling this force is explained completely in Ref. [41], and interested readers can refer to it. This force can be computed as follows:

$$\vec{F}_{\text{ext}}^k = -\rho \left(1 + \alpha_1^2\right)^{\frac{3}{2}} A^2 \omega^2 k_i \, \exp 2(k_i x + \alpha_1 k_i y) \left[\sin\theta_R \vec{i} + \cos\theta_R \vec{j} \right], \tag{14}$$

where A is SAW amplitude and ω is an angular frequency which is related to SAW frequency, f, via $\omega = 2\pi f$. Moreover, α_1 is the attenuation coefficient, k_i is the wave number, and θ_R is the radiation (Rayleigh) angle.

In order to apply external body forces, the term $\overline{F}_i$ is added to Eq. (3):

$$\overline{F} = M^{-1}\left(I - \frac{1}{2}S\right)M\tilde{F}, \tag{15}$$

where I is a 9×9 unit matrix and $\tilde{F}$ is as follows:

$$\tilde{F}_i = w_i\left[3(\vec{c}_i - \vec{u}) + 9(\vec{c}_i \cdot \vec{u})\vec{c}_i\right] \cdot \vec{F}, \tag{16}$$

where $\vec{F}$ is the body force.

In this study, periodic and no-slip boundary conditions are used. Indeed, the periodic boundary condition applies to the transformation step. For this purpose, the particles that leave on one boundary are reintroduced on the opposite side of the simulation domain. No-slip boundary condition is applied at the solid wall using a simple bounce-back scheme. The contact angle θ is enforced on the wall through the modified [40] geometrical formulation proposed by Ding and Spelt [44].

2.1 Simulation setup

Two droplets with a certain diameter and contact angle are loaded on the path taken by a SAW propagating through the substrate (Fig. 1). Density and viscosity ratios are 1000 and 15, respectively, and the surface tension coefficient is 0.072 N/m [45]. The no-slip boundary condition is implemented on the substrate and the upper side. The periodic boundary condition is applied to the other sides. The schematic of the problem is presented in Fig. 1.

3 Results and discussions

The obtained results are presented here. At first, the verification of numerical simulation is studied. Then, the main physics is illustrated.
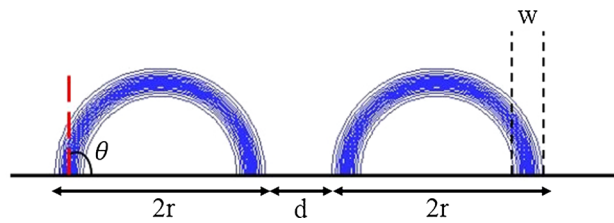
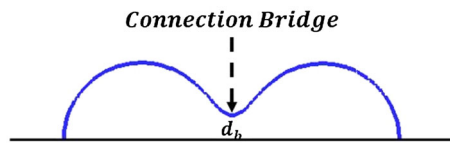**Fig. 2** Schematic of the problem

Fig. 3 Connection bridge radius

3.1 Verification results

For verification of simulation, the coalescence phenomena near the substrate are firstly studied. Then, a single droplet subjected by SAWs is presented. All results are compared with reliable and available numerical and experimental data. So, we can conclude that the numerical procedure is proper for studying the intended problem.

3.1.1 Coalescence phenomena

The coalescence of droplets is a phenomenon which arises in many multi-phase flow applications such as sintering, separation, and microfluidics [4]. In this situation, two droplets merge together and a bigger droplet is formed [5]. From a physical point of view, this is described with the minimization of surface energy. In this section, we investigate the coalescence of two droplets located on a solid substrate.

The flow parameters used for the simulation of coalescence phenomena are shown in Fig. 2. The distance between two droplets (d) and the interface width (w) are the most important parameters and determine the conditions of the coalescence. The diameter of the droplets is $2r$ and the contact angle is set to be θ. Calculations are performed in a rectangular domain with 401×201 uniform mesh. Periodic boundary conditions are applied on the open boundaries and the geometrical wetting boundary condition and the bounce-back boundary condition are used on the other boundaries.

When the coalescence phenomenon starts and two droplets come in contact with each other, a connection bridge is first formed between them. This parameter is another important one in our study. The schematic of the coalescence and the connection bridge radius (d_m) are presented in Fig. 3.

First, two droplets with contact angle $\theta = 90°$ in three different positions are assumed: $d/w = 1.1$, 1.8, and 3.2. The time evolution of droplets is shown in Fig. 4. We can observe that if $d/w > 2$, the coalescence does not happen. With this point of view, our results are similar to the numerical results presented by Zheng et al. in Ref. [46]. Also, t_0 (the time when the phenomenon is started) is presented in Table 1. As we expect, it can be shown that when the distance between two droplets is reduced, the coalescence time will be reduced.

Variation of d_m/r versus $t-t_0$ is presented in Fig. 5. Based on the results obtained by Reis and Phillips [47], the final radius of the droplet will be equal to $\sqrt{2}r$. So, the parameter d_m/r must approach $\sqrt{2}$ and the numerical results show this value.

Ristenpart et al. [6], based on inviscid considerations, developed an analytical relation for variation of connection bridge:

$$d_m \sim \left(\frac{\sigma h_0^3}{\mu R_0^2} \right)^{1/2} \sqrt{t}, \tag{17}$$

where σ is surface tension coefficient, h_0 is the initial height of droplet, μ is viscosity coefficient, and R_0 is the droplet radius. Therefore, we can show that in our problem $\frac{d_m}{r} \sim \left(\frac{\sigma}{R_0 \mu} \right)^{1/2} \sqrt{t}$. This analytical solution is compared with the numerical results in Fig. 5. Albeit, the analytical solution in the steady condition is not valid due to inviscid considerations. We can observe that the numerical results follow the analytical solution with a relatively good accuracy. In Fig. 5, the maximum error is about 16%.

Then, the effect of hydrophobicity on the coalescence is investigated. For this purpose, a hydrophilic surface with contact angle $\theta = 27°$ and a hydrophobic surface with $\theta = 120°$ are considered. In order to compare the numerical results with the available experimental data, these contact angles have been considered. Results show that in order to start the coalescence phenomenon on a hydrophobic surface, the distance between two droplets must be reduced to about $d/w \approx 1.0$. On the other hand, on hydrophilic
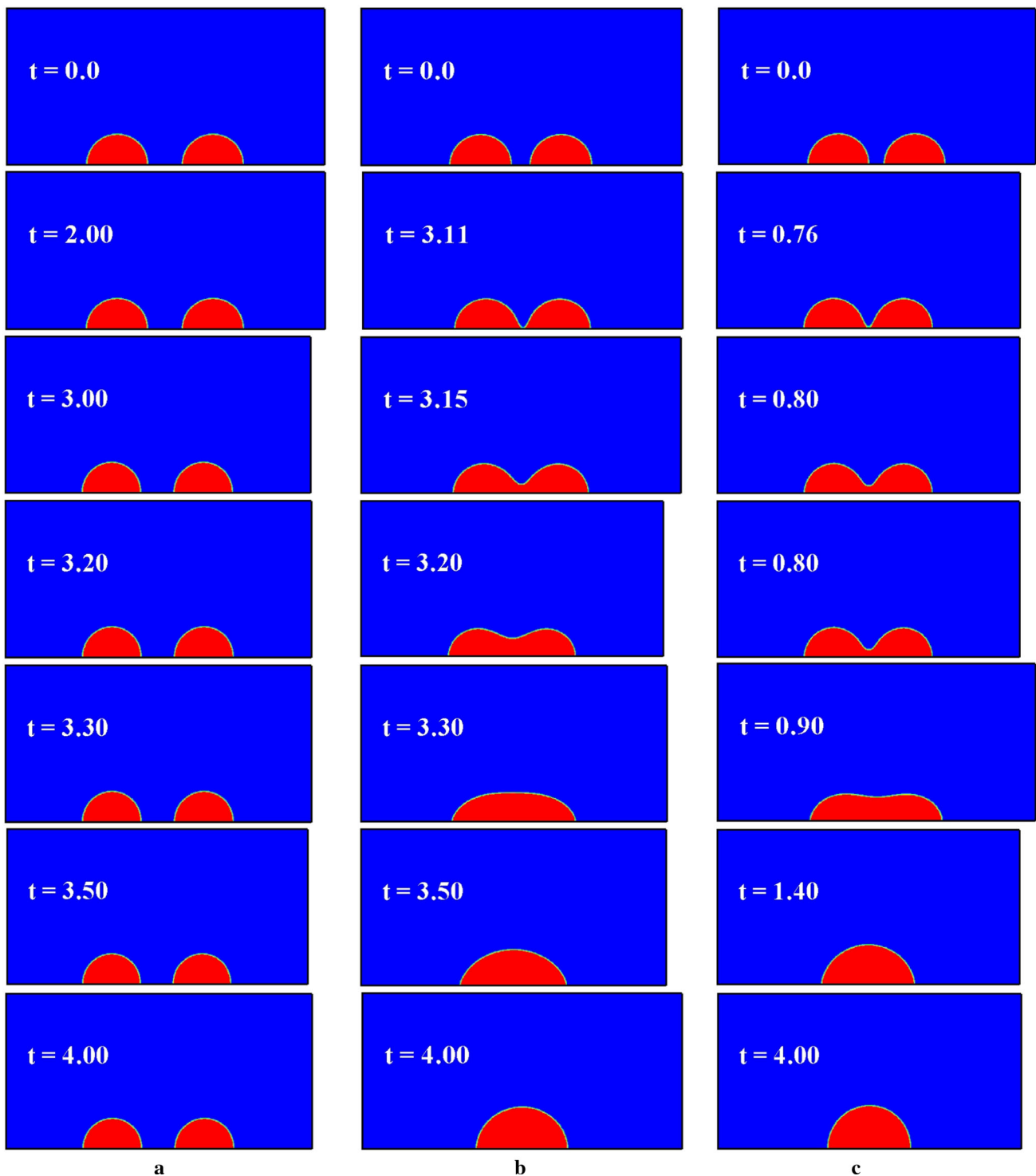
Fig. 4 Time evolution of the droplets located in different distances: **a** $d/w = 3.2$, **b** $d/w = 1.8$, and **c** $d/w = 1.1$

surfaces, if $d/w < 3.0$, we can observe the coalescence. The time evolution of droplets in these conditions are presented in Figs. 6 and 7 (for hydrophilic and hydrophobic surface, respectively), and the numerical results are compared with experimental data.

The variation of d_m as a function of time is illustrated in Fig. 8 for $\theta = 27°$ and $120°$. The time of starting of coalescence is 0.12 s for hydrophobic surface and 1 s for hydrophilic surface. Therefore, we can conclude that if θ is increased, d/w in which the coalescence is started is reduced. In other words, droplets have more tendencies to coalesce on the hydrophilic surfaces. Also, by increasing the θ, the steady value of d_m/r is increased. Also, by increasing the θ, the time to reach the steady d_m/r is decreased, and

Table 1 Time of starting the coalescence at different distances

d/w	t_0
1.1	0.76
1.8	3.11

in other words, the minimization of the surface energy happens faster on hydrophobic surfaces. Note that based on results presented in Ref. [48], in the coalescence of two droplets in a periodic domain, before two droplets merge to become a single droplet, some oscillations are generated at the surface of the droplet, which ensure that the effects of surface tension are properly implemented in the numerical method. When we investigate the coalescence of sessile droplets, these oscillations are appeared as step-like behaviors. So, when the rate of minimization of surface energy increases, these behaviors are damped faster.

The reason to the coalescence phenomenon is the minimization of surface energy. When two droplets are coalesced and one droplet is formed, the surface area is decreased and with respect to fixed surface tension coefficient, surface tension force is decreased. The surface area on a hydrophilic substrate is the minimum and so, the tendency to coalesce is increased, while this coalescence reaches a steady state in a long duration of time.

3.1.2 Droplet manipulation using SAW

In this section, we want to verify the modeling of the effects of SAWs on droplet dynamics. For this purpose, the valuable experimental data presented by Wang et al. [49] are used. Acoustofluidics along surfaces based on AlN/Si is investigated in this reference where the wavelength of this substrate is 64 microns and the radiation angle is 16.9°.

At first, the pumping mode is considered; the wave frequency is set to 80.35 MHz, and for some wave amplitudes, the numerical results are compared with experimental data (Fig. 9 and Table 2). Also, with a wave amplitude of 7.19 nm, the jetting mode is simulated and compared with experimental data in Fig. 10. These results show that the numerical modeling is relatively close to the experimental data. Also, we performed a perfect investigation on this problem in our previous works such as [41–43, 50] and interested readers can refer to them.

In the previous section, we presented the coalescence phenomena and compared our results with reliable numerical and experimental data. In the present section, we investigated the dynamical behaviors of droplet affected by SAW, while in our previous works, these phenomena were completely presented, too. Therefore, it can be inferred that the study of the phenomenon, which involves the combination of the two mentioned problems, can be performed based on the developed numerical method with acceptable accuracy. So, this physics is studied in the next section.

3.2 Coalescence affected by SAW

The active control of droplets coalescence dynamics using SAW is the purpose of this work. Dynamical behaviors of droplets and different parameters such as contact time, coalescence time, maximum spreading, and the velocity of moving droplets can be
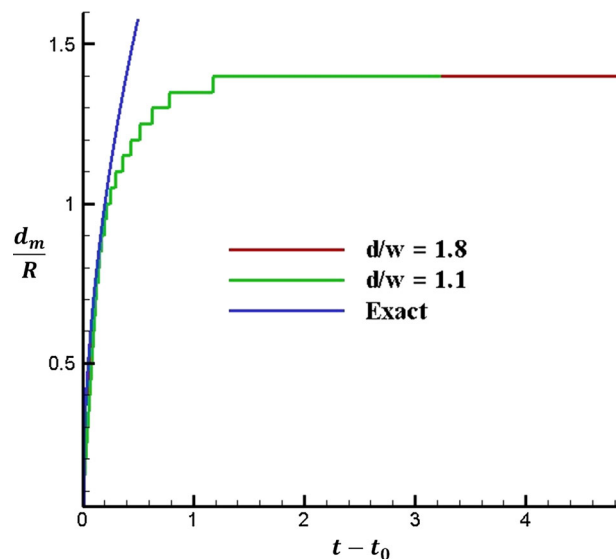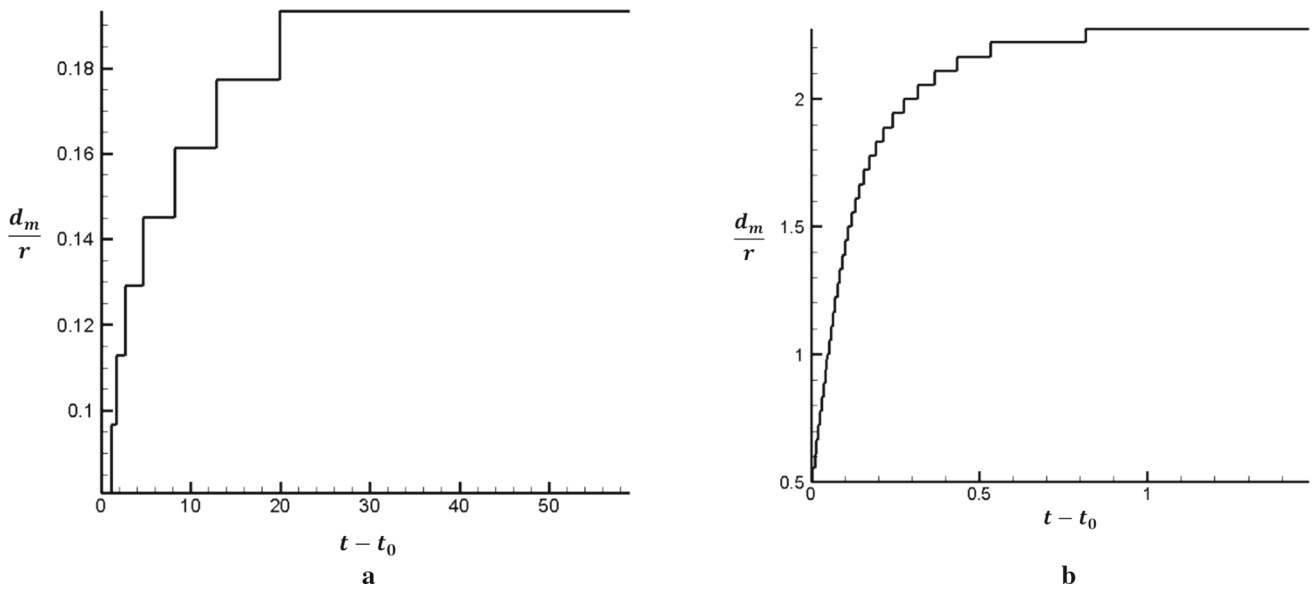

Fig. 5 Variation of connection bridge as a function of time
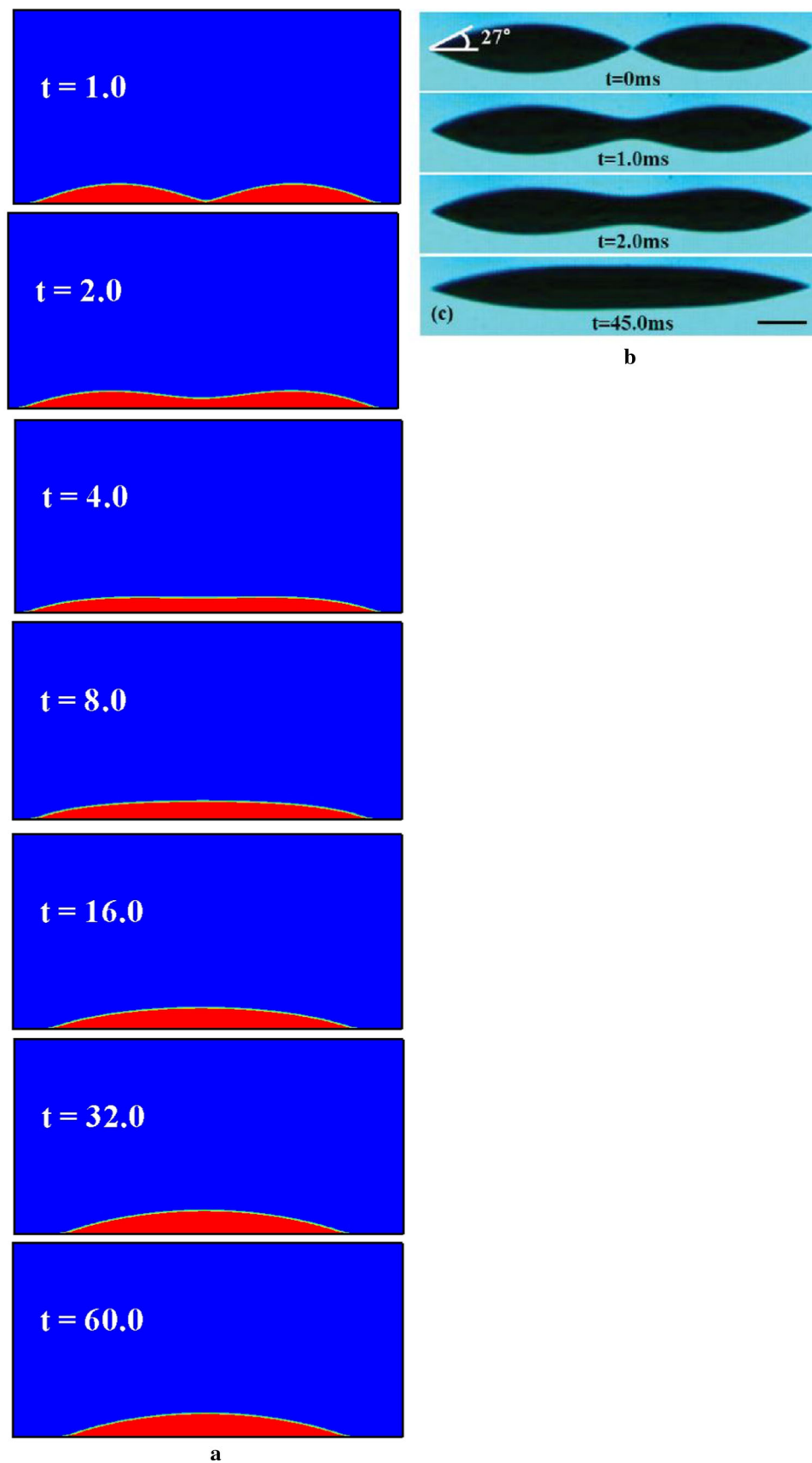
Fig. 6 Coalescence phenomenon on a hydrophilic surface: **a** numerical results and **b** experimental data [5]
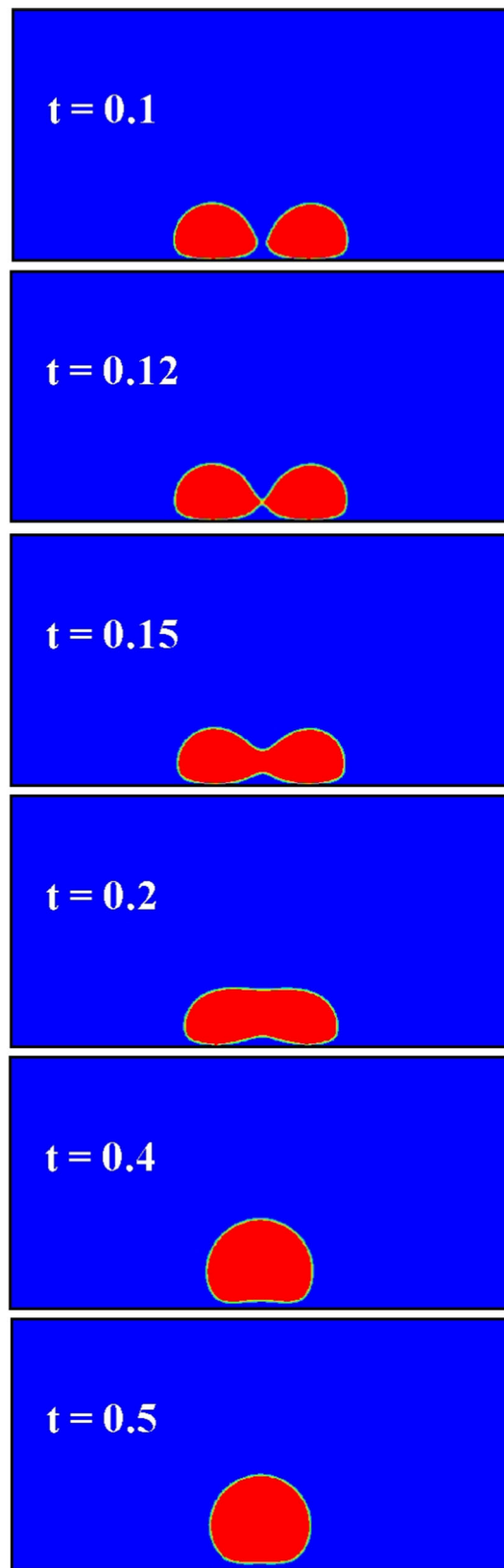
Fig. 7 Coalescence phenomenon on a hydrophobic surface

Fig. 8 Effect of hydrophobicity on connection bridge: **a** $\theta = 27°$ and **b** $\theta = 120°$

Fig. 9 Droplet shape in pumping mode: **a** experimental data presented by Wang et al. [49] and **b** numerical results

Table 2 Comparison of droplet velocity with experimental data	A (nm)	Experimental velocity of moving droplet (mm/s)	Numerical velocity of moving droplet (mm/s)
	3.51	20	23.2
	4.07	30	31
	4.6	40	39.8

affected by SAW in coalescence phenomena. Before investigating the results, we examine the dynamics of the phenomenon with a force diagram (Fig. 11). As stated, when two droplets are located at a certain distance, they merge together. So, we can consider that an interfacial force (coalescence force) acts on the droplets and moves them. The SAW force is applied to flow control and with definition, it is a body force that is exponentially reduced in space and acts on the contact point of the droplet. Because the wavelength is smaller than the droplet radius, the energy of the wave is completely transferred to the first droplet. F_{SAW} has two components: F_{SAWx} which is superimposed to coalescence force, and F_{SAWy} which is normal to the surface and is opposed to surface tension force. When F_{SAWy} overcomes surface tension force, the droplet is broken and even detached from the surface.

With respect to the parameters presented in Fig. 2, two distributions of the droplets are considered and illustrated in Fig. 12. These two situations are $d/w = 1.1$ and 3.2. For generation of droplets, firstly, the static droplet is solved, and then, using the translation and the copy of droplets, they are loaded on the surface at the certain places.

When we want to study the problems such as coalescence phenomena, one approach is related to probability balance equations (PBE). For example, the state of distribution of a population, such as size, is considered, and related transport equations are investigated based on PBE [51]. So, the knowledge about the distribution of shape, size, composition, etc., for the droplets is so important to present accurate transport equations [52]. Using droplet distribution function, we can compute the fluid properties, and simulate the flow field (for example with CFD). Also, in order to understand thermodynamics, especially in problems that thermodynamic equilibrium cannot be considered or about non-Newtonian fluids, thermo-statistical distribution functions are one of the useful tools [53].

In the physics, the distribution function of a system is a seven-variable function such as $f(x, y, z, t, u, v, w)$ which gives the number of particles that are near the position (x, y, z) and have velocity (u, v, w), at time t [54]. The distribution function is specialized with respect to a certain coordinate, and in some references, it is named cumulative distribution function [55]. Also,
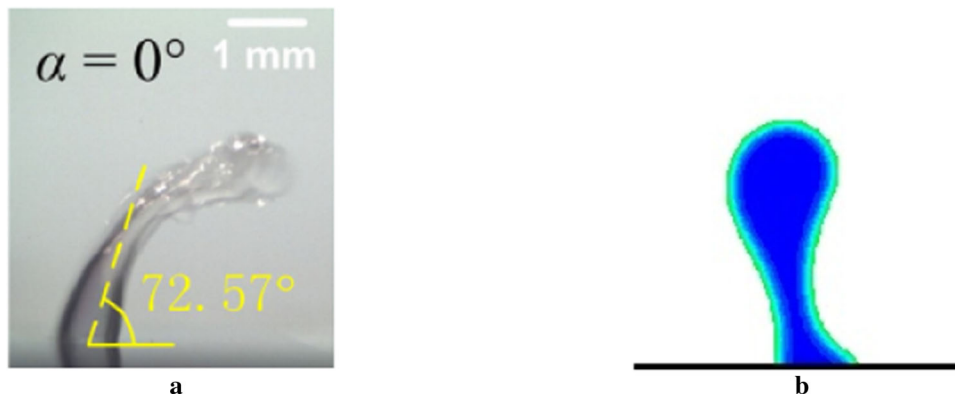
Fig. 10 Droplet shape in jetting mode: **a** experimental data presented by Wang et al. [49] and **b** numerical results
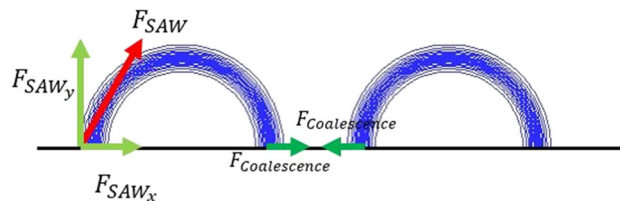

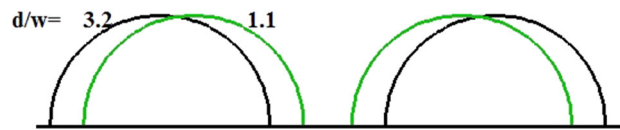**Fig. 11** Force diagram of coalescence phenomena subjected to SAW

Fig. 12 Distribution of droplets

every distribution function is increasing and right-continuous function, and its limits at minus infinity and positive infinity satisfy 0 and 1, respectively [56]. Based on normal distribution, distribution function is defined as follows:

$$f = n\left(\frac{m}{2\pi KT}\right)^{\frac{3}{2}} \exp\left(-\frac{m(u^2 + v^2 + w^2)}{2KT}\right),$$

(18)

where K is Boltzmann constant, T is temperature, n is density number, and m is particle mass. When the thermodynamic equilibrium is considered, distribution function is named Maxwellian.

In general, the shape of droplet distribution function is modeled as lognormal, Rosin–Rammler, and non-fundamental and determines size, mass, and range of density for droplets. These models are compared in Ref. [57], and the choice of each has been examined for different issues. Note there are two major classes of droplet distribution function models: (1) correlations models and (2) detailed simulation models. The first one relies on non-dimensional parameters such as Reynolds number or Weber number, whereas the second class is based on computation of differential equations for equilibrium and transition of droplet size. For more details, interested readers should refer to [52].

The dynamical behaviors of droplets can be classified in two main modes: pumping and jetting. In the pumping mode, droplets are moved with SAW and the detachment of them is not observed, while in the jetting mode, the droplets (separately or droplet formed after coalescence) are broken down and detached portions of them are formed. At first, we study the pumping mode.

We presented the important parameters which describe the interaction of SAW and droplet in Ref. [50]. In this work, the effects of wave frequency (f) and SAW amplitude number (A_{SAW}), which is defined as follow, are considered:

$$A_{SAW} = \frac{A\rho\sigma}{\mu^2},$$

(19)

where A is the wave amplitude and ρ is the density of the fluid. At first, the frequency of 64.5 MHz and $4 < A_{SAW} < 33$ are considered and droplets are located at a distance of $d/w = 1.1$ and 3.2. (We know that when $d/w < 2$, the coalescence phenomenon happens naturally.) Note that in this frequency and range of A_{SAW} just the pumping mode is observed.

Time evolution of dynamical behaviors of droplets when $d/w = 1.1$ and $A_{SAW} = 14.8$ are presented in Fig. 13. SAW moves the first droplet and when two droplets coalesce, the formed droplet continues moving subjected to waves. The main importance of these dynamical behaviors is in the case of $d/w = 3.2$; using SAW, we could coalesce the droplets.
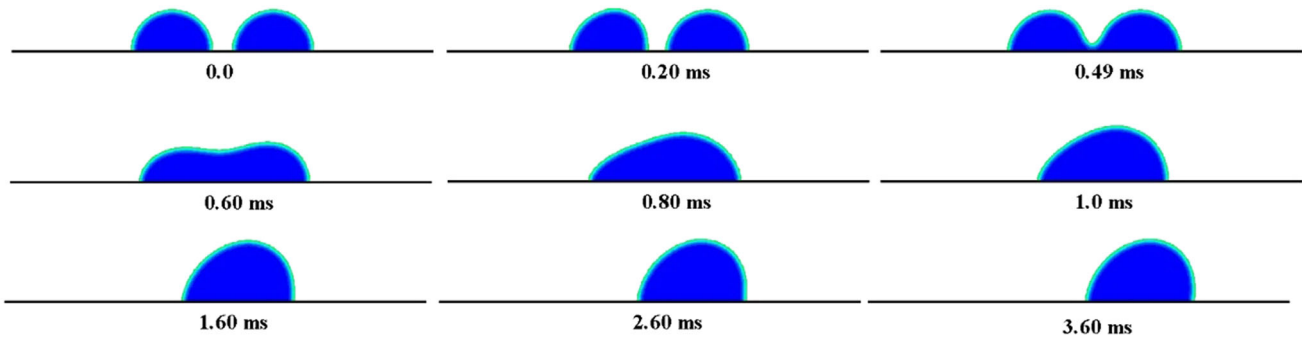
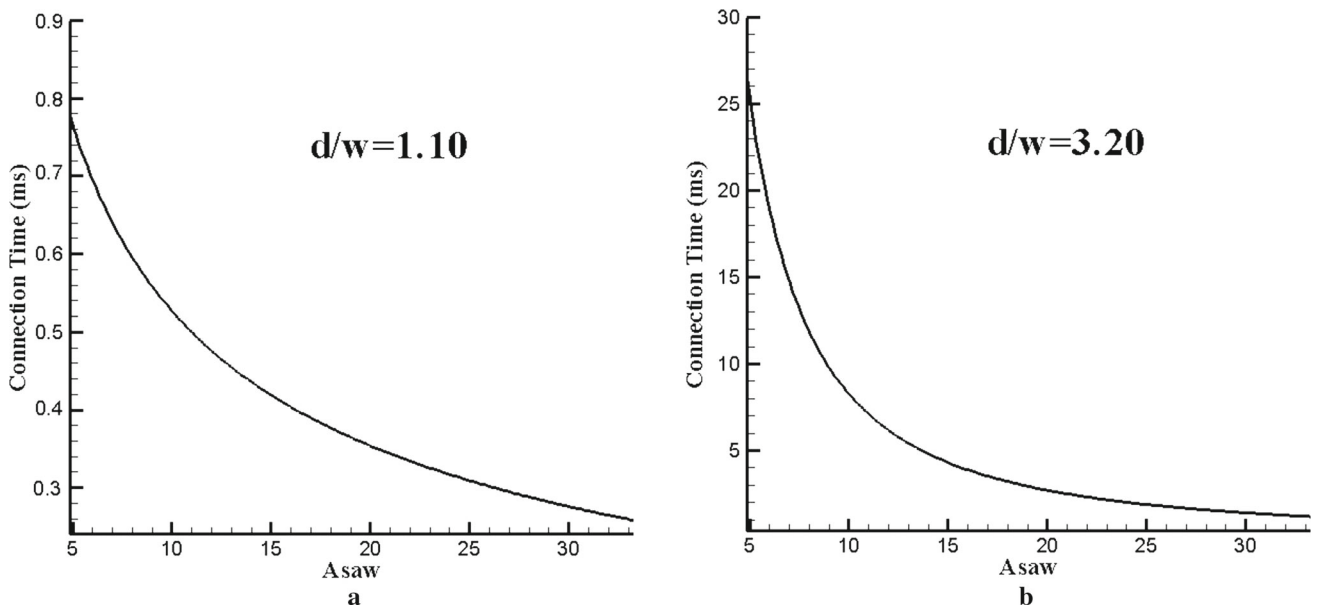**Fig. 13** Dynamical behaviors of coalescence phenomena affected by SAW in the pumping mode

Fig. 14 Connection time affected by SAW: **a** $d/w = 1.1$ and **b** $d/w = 3.2$

The effect of SAW on the connection time is presented in Fig. 14. At $d/w = 1.1$, the connection occurs after 0.76 ms, and this time can be reduced by SAW. Also, when $d/w = 3.2$, the coalescence phenomena are observed by applying the SAW, while at this distance, the droplets did not coalesce together. Additionally, these diagrams show that by increasing the wave amplitude the connection time is decreased because the energy transferred to the first droplet has been increased.

The coalescence time as a function of A_{SAW} is illustrated in Fig. 15. With these results, the coalescence time firstly decreases, and by increasing A_{SAW}, it is increased. As explained before, the coalescence phenomena occur to minimize the surface energy. When the wave amplitude is increased, the kinetic energy of droplets is increased, and they coalesce together quickly. However, when A_{SAW} is greater than about 16, the dynamical behaviors of droplets subjected to SAW overcome the behaviors of coalescence phenomenon and the minimization of the surface energy becomes difficult and so, the time required to form the steady shape of the final droplet is increased.

In order to discuss the acoustofluidic mechanism, notice that the wave transfers the energy to the droplet. This energy transfer leads to a faster droplet motion and completion of the coalescence phenomena in the shorter duration of time interval, while the volume of fluid increases after coalescence. Until $A_{SAW} \sim 16$, the energy level (compared to the volume of the formed droplet) is not significantly increased and so, the coalescence time is reduced. But, from $A_{SAW} \geq 16$, the energy level compared to volume of droplet is increased, and the minimization of the surface energy occurs in the longer time interval, and so the coalescence time begins to increase.

The shape of the formed droplet is investigated in Fig. 16. Note that in this figure, the maximum height of the droplet and the wetting length were normalized by the radius of a single droplet. By increasing the A_{SAW}, the droplet height is increased, and this is the effect of the F_{SAWy} in Fig. 11. Therefore, the wetting length is reduced and the droplet reaches a shape that can be moved by SAW.
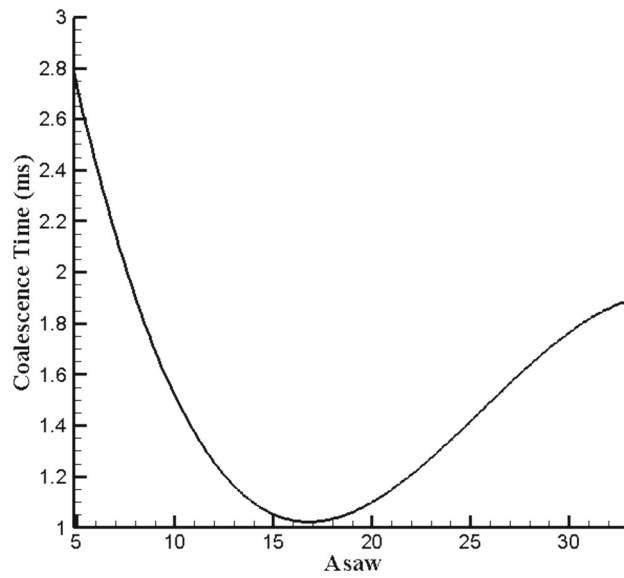
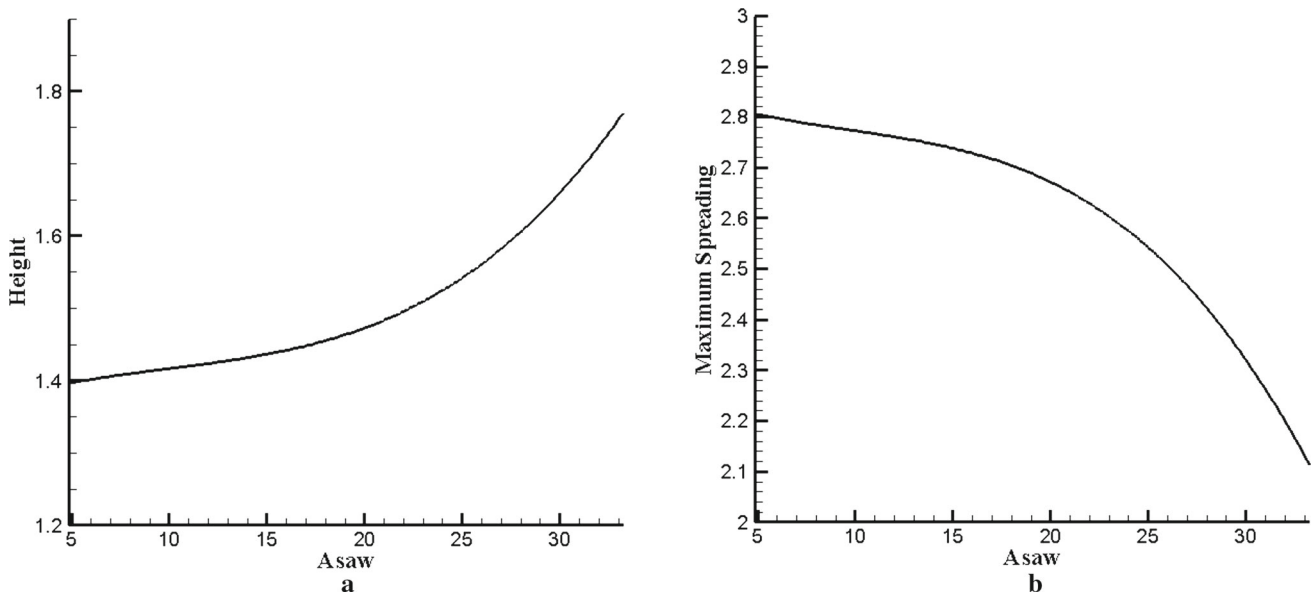**Fig. 15** Effect of SAW on the coalescence time

Fig. 16 Variation of droplet shape: **a** non-dimensional droplet height and **b** non-dimensional wetting length

Reynolds number (Re) versus A_{SAW} is investigated in Fig. 17. This parameter is defined as follows:

$$\text{Re} = \frac{\rho u l}{\mu}, \tag{20}$$

where l is the characteristic length and is considered as the droplet radius and u is the velocity of the moving droplet. In this figure, the solid, dash-dot, and dash lines are for $d/w = 1.1$, $d/w = 3.2$, and formed droplet, respectively. First, we can observe that the droplet moves faster when the wave amplitude is increased. The second and more important result is that the droplet which is located in the distance of $d/w = 1.1$ moves faster than the other one. In the distance of $d/w = 1.1$, the coalescence force is applied on the droplet, in addition to the tangential component of acoustic force. The superposition of these two forces moves the droplet too fast.

To investigate the jetting mode, we set the wave frequency equal to 271 MHz in our numerical laboratory. In this condition, three different dynamical behaviors are observed and presented below. Also, the detachment efficiency parameter is defined in order to study the performance of the SAW in this mode. It is important to note that the distance d/w does not change the dynamical behaviors in the jetting mode and the differences occur only in the time intervals of events.
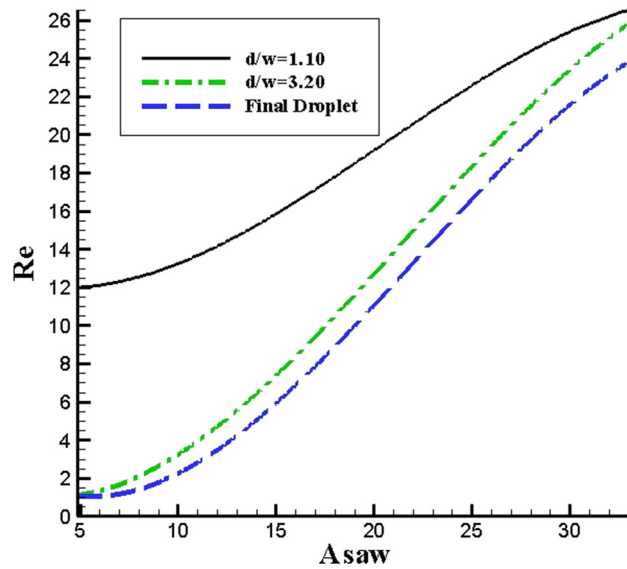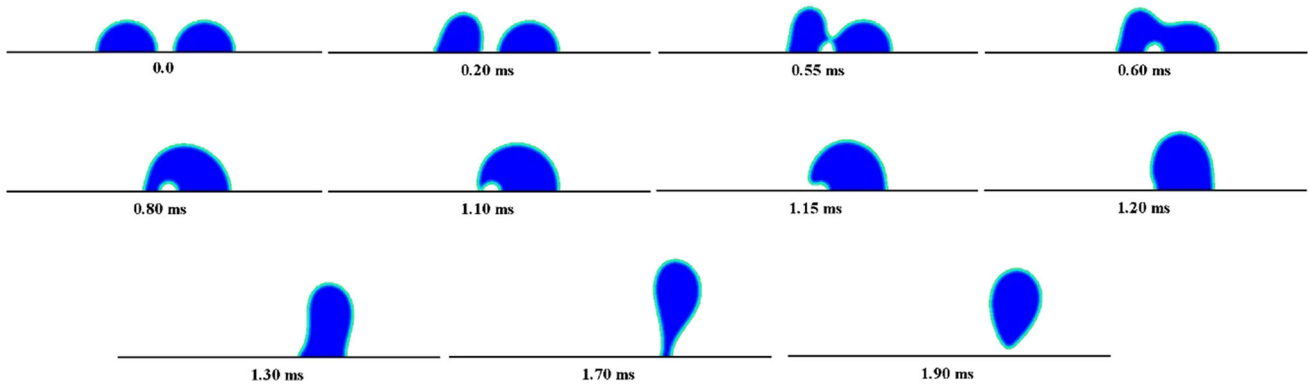
Fig. 17 Re–A_{SAW} diagram

Fig. 18 First dynamical behaviors of coalescence phenomena affected by SAW in the jetting mode

The first dynamics of jetting is related to $A_{SAW} < 8$. In this situation, the height of the first droplet is increased, affected by SAW. Then, at a point above the substrate, connection of two droplets occurs. So, two droplets coalesce together and the wave energy causes the formed droplet to detach from the surface (Fig. 18).

The second dynamics occurs when $8 < A_{SAW} < 10$ and the time evolution of behaviors of droplets is illustrated in Fig. 19. We observe that droplets show periodic behaviors: the first droplet affected by SAW is detached from the surface, then the waves reach the second droplet. This droplet begins the jetting process and a vortical field is generated near the surface (Fig. 20). The detached droplet places in the vortical field and, while it is affected by the vorticities, it places on the substrate again. So, the phenomena are repeated and, in this situation, no mass is actually detached from the surface.

Finally, the third dynamical behaviors are presented in Fig. 21. In this situation, the wave energy is enough to detach two droplets (completely or a portion of them) from the wall. For these conditions, A_{SAW} must be greater than 10.

In this section, we want to make a comparison between different wave amplitudes in order to investigate the performance of using SAW to remove the droplets from the surface. For this purpose, we define the detachment efficiency parameter as the removed mass from the surface (m) per unit time stand for detachment of droplet (t). Note, we normalize the removed mass by the sum of the mass of two initial droplets, namely $m_{01} + m_{02}$ (indices of 1 and 2 are related to the first and the second droplets, and 0 denotes the initial condition) and time by wave frequency and so, this parameter is a non-dimensional quantity and it is defined as, $\frac{m}{t} \frac{1}{(m_{01}+m_{02})f}$.

The variation of the detachment efficiency parameter versus A_{SAW} is presented in Fig. 22. At first, because the dynamical behaviors are an approach to the second dynamics, this parameter is reduced. Then, by increasing the wave amplitude, the removed mass is increased and the time of jetting is reduced and so, the detachment efficiency parameter is increased until near A_{SAW} equal to 14. When $A_{SAW} > 14$, the detachment time is decreased by increasing the wave amplitude, but the removed mass is decreased, too.

This physics is shown in Fig. 23, and its reason is related to the normal component of surface acoustic wave force. The rate of increase in F_{SAW_y} is such that it causes a sudden increase in the height of droplet and as a result, a portion of the mass is separated
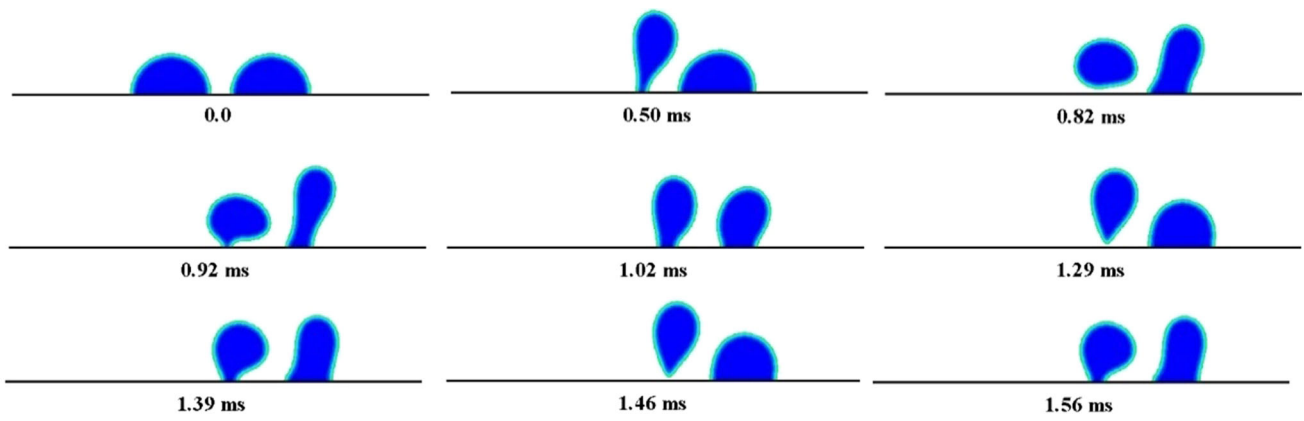
Fig. 19 Second dynamical behaviors of coalescence phenomena affected by SAW in the jetting mode
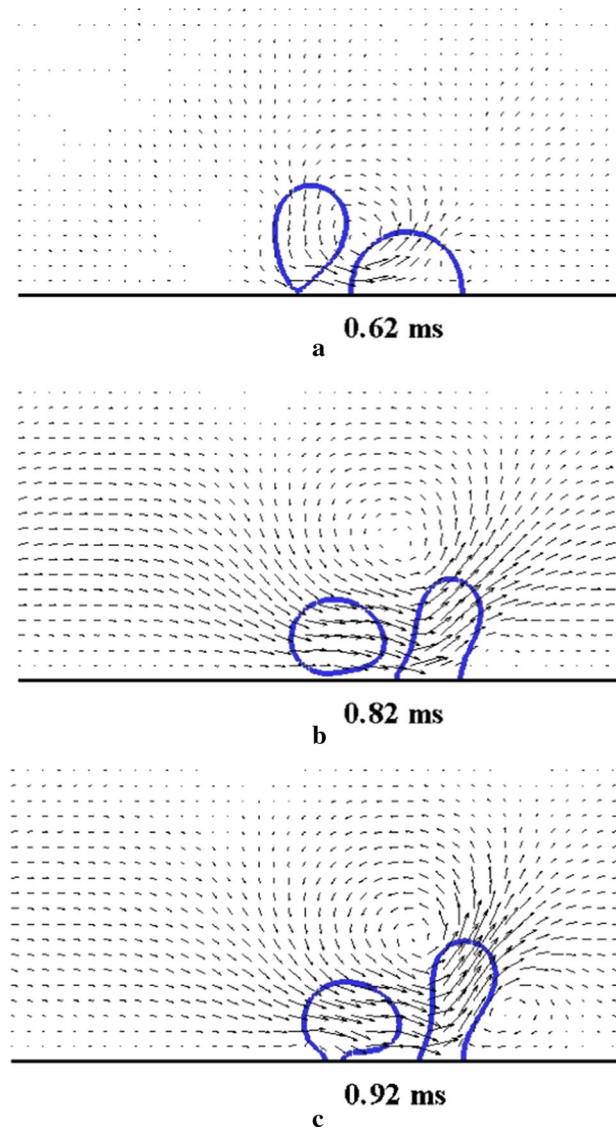
Fig. 20 Velocity field near the droplets

from the main droplet. Therefore, a great amount of the mass (relative to previous conditions) remains on the wall and the detachment efficiency parameter is decreased.
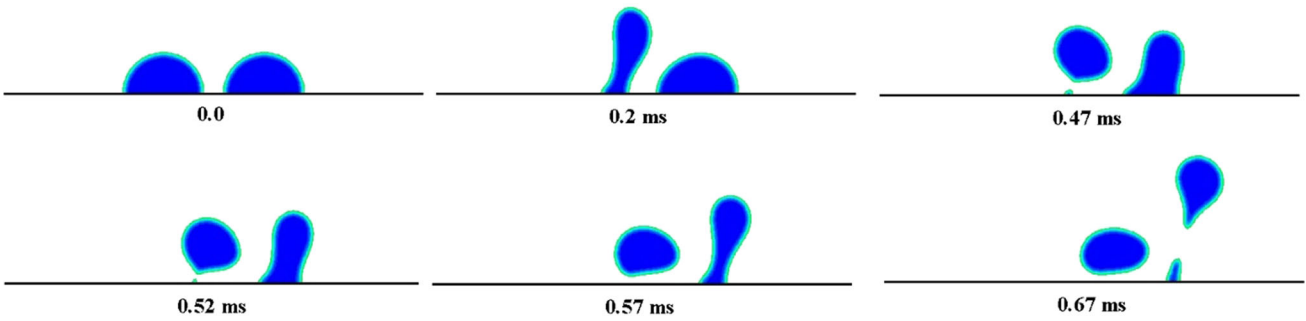
Fig. 21 Third dynamical behaviors of coalescence phenomena affected by SAW in the jetting mode
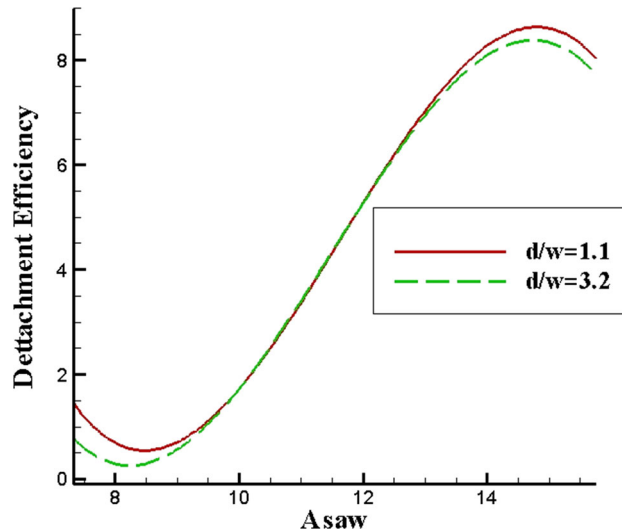

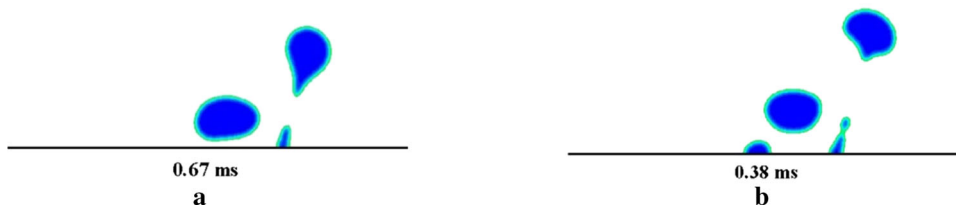**Fig. 22** Variation of detachment efficiency parameter

Fig. 23 Comparison of the amount of removed mass: **a** $A_{SAW} = 11.5$ and **b** $A_{SAW} = 15.8$

To discuss about optimality of $A_{SAW} = 14$ for removing droplets from the surface, note that, the detachment efficiency is defined based on the time at which the first portion of droplet is removed. Also, the jetting phenomena occur based on a comparison of the magnitude of F_{SAW_y} and the surface force ($F_{surface}$), which is related to surface tension (when $F_{SAW_y} > F_{surface}$, dynamical behaviors of droplet is in the jetting mode). In the situations of $A_{SAW} > 10$, by increasing wave energy, component of F_{SAW_y} increases (compared to $F_{surface}$), and so more mass in shorter duration of time is removed that leads to an increase in detachment efficiency. When $A_{SAW} > 14$, the energy transferred to the fluid is so much and $F_{SAW_y} \gg F_{surface}$. In this situation, the dynamical behaviors of droplet are on the verge of atomization mode. This leads to the detachment of a small portion of fluid from the droplet, near the surface, whereas with passing of time, the largest portion of droplet is detached, but based on definition (presented in this article), because the first removed mass of droplet is reduced, the detachment efficiency is reduced. Note that, because of limitation in developed code, the atomization mode cannot be investigated.

For explaining the physical insights, note that when two droplets are located at the distance of $d/w > 2$, they do not coalesce, whereas when $d/w < 2$, the coalescence is observed. When the SAW reaches to the first droplet (based on the direction of wave propagation), due to viscosity, the energy of wave is transferred to the droplet and so, it begins to move and coalesces with adjacent droplet. When $d/w > 2$, this is so important. Based on transfer of the energy, the droplet may be jetted, which was investigated in three different ranges of A_{SAW} (a parameter that describes the wave energy) in this research.

4 Conclusion

In this paper, the coalescence of two same droplets subjected to surface acoustic waves has been simulated by the multi-relaxation time color gradient model of Lattice Boltzmann method. The acoustic force has been implemented as an external body force.

At first, the coalescence of two droplets located on a substrate was investigated, and the obtained results were compared with reliable results. Based on the findings, when the contact angle θ was equal to $90°$, two droplets located at a distance of $d/w > 2$ did not coalesce. Also, when the distance of two droplets was reduced, the connection time was reduced as well. We showed that the connection bridge, with respect to the time, followed a power law with a $1/2$ exponent up to a threshold time, and beyond that time, it approached a constant value. The hydrophobicity in these phenomena was studied, too. We concluded that if θ was increased, d/w, in which the coalescence was started, was reduced. In other words, droplets had more tendencies to coalesce on the hydrophilic surfaces. Also, by increasing the θ, the steady value of d_m/r was increased. By increasing the θ, the time to reach the steady d_m/r was decreased.

Then, the effects of SAWs on the physics of coalescence were illustrated. For analyses of the results, we considered a coalescence force which was implemented in the force diagram of the problem. Because the wavelength is smaller than the radius of droplets, the acoustic force was only affected on the first droplet. We observed that even in the distance of $d/w > 2$, two droplets coalesced, and using SAWs, we could control the dynamical behaviors of the droplets. The connection time was reduced when the wave amplitude was increased.

The dynamical behaviors of droplets subjected to SAW overcame the behaviors of the coalescence phenomenon and the minimization of the surface energy became difficult and so, the coalescence time was increased. By increasing the wave amplitude, the height of the final droplet was increased and the wetting length was reduced.

In the jetting mode, three different dynamical behaviors were observed: 1—the coalescence of two droplets and the detachment of the formed droplet for $A_{SAW} < 8$, 2—periodic detachment and connection of droplets for $8 < A_{SAW} < 10$, and 3—detachment of two droplets for $A_{SAW} > 10$. With a definition of detachment efficiency parameter, we showed that $A_{SAW} \approx 14$ is optimum for the removal of the droplets from the surface.

This study can be applicable in the problems that they are based on coalescence phenomena (such as demulsifier of water from crude oil, spray coating, and heat transfer in the spray cooling), in order to strengthen the intended phenomena. For example, the connection time was reduced, using SAW, and it is important for increasing the mixing efficiency. Another application is removal of droplets from the surfaces, which can be used in anti-icing devices [58]. As one scenario, the droplets can be collected on the surface and then remove the formed droplet. For future works, we can consider the distribution of droplets with different sizes, or more importantly, having a layer of liquid and analyze its formation and emission of droplets. This last case would be more relevant to removing a layer of water from the surfaces.

Data Availability Statement This manuscript has associated data in a data repository. [Authors' comment: The authors confirm that the data supporting the findings of this study are available within the article.]

Declarations

Conflict of interest The authors declare that there is no conflict of interest.

References

1. P.G. De Gennes, Wetting: statics and dynamics. RMP **57**, 3 (1985)
2. A.L. Yarin, Drop impact dynamics: splashing, spreading, receding, bouncing. Annu. Rev. Fluid Mech. **38**, 1 (2006)
3. M.A. Fardin, M. Hautefeuille, V. Sharma, Spreading, pinching, and coalescence: the Ohnesorge units. *Soft Matter* **11** (2022)
4. Y. Sui, M. Maglio, P.D. Spelt, D. Legendre, H. Ding, Inertial coalescence of droplets on a partially wetting substrate. Phys. Fluids **25**, 10 (2013)
5. M.W. Lee, D.K. Kang, S.S. Yoon, A.L. Yarin, Coalescence of two drops on partially wettable substrates. Langmuir **28**, 8 (2012)
6. W.D. Ristenpart, P.M. McCalla, R.V. Roy, H.A. Stone, Coalescence of spreading droplets on a wettable substrate. PRL **97**, 6 (2007)
7. Y.B. Erkan, *Numerical Simulation of Coalescence of Micron-Submicron Sized Droplets and Thin Films* (Middle East Technical University, 2021)
8. W. Liu, N. Li, Z. Sun, Z. Wang, Z. Wang, Binary droplet coalescence in shear gas flow: a molecular dynamics study. J. Mol. Liq. **354**, 118841 (2022)
9. Y.S. Tian, Z.Q. Yang, S.T. Thoroddsen, E. Elsaadawy, A new image-based microfluidic method to test demulsifier enhancement of coalescence-rate, for water droplets in crude oil. J. Pet. Sci. Eng. **208**, 109720 (2022)
10. T.M. Ho, A. Razzaghi, A. Ramachandran, K. Mikkonen, Emulsion characterization via microfluidic devices: a review on interfacial tension and stability to coalescence. Adv. Colloid Interface Sci. **299**, 102541 (2022)
11. I. Adeyemi, M. Meribout, L. Khezzar, N. Kharoua, K. AlHammadi, Numerical assessment of ultrasound supported coalescence of water droplets in crude oil. Ultrason. Sonochem. **88**, 106085 (2022)
12. C. Liu, M. Zhao, Y. Zheng, L. Cheng, J. Zhang, C.A. Tee, Coalescence-induced droplet jumping. Langmuir **37**, 3 (2021)
13. C. Liu, M. Zhao, Y. Zheng, D. Lu, L. Song, Enhancement and guidance of coalescence-induced jumping of droplets on superhydrophobic surfaces with a U-groove. ACS Appl. Mater. Interfaces **13**, 27 (2021)

14. M. Miot, G. Veylon, A. Wautier, P. Philippe, F. Nicot, F. Jamin, Numerical analysis of capillary bridges and coalescence in a triplet of spheres. Granul. Matter **23**, 3 (2021)

15. S. Feng, L.I. Yi, L. Zhao-Miao, C. Ren-Tuo, W. Gui-Ren, Advances in micro-droplets coalescence using microfluidics. Chin. J. Anal. Chem. **43**, 12 (2015)

16. X. Huang, L. He, X. Luo, K. Xu, Y. Lü, D. Yang, Convergence effect of droplet coalescence under AC and pulsed DC electric fields. Int. J. Multiph. Flow **143**, 103776 (2021)

17. S.C. Lin, X. Mao, T.J. Huang, Surface acoustic wave (SAW) acoustophoresis: now and beyond. Lab Chip **12**, 16 (2012)

18. V. Aleksandrov, S. Kopysov, L. Tonkov, Vortex flows in the liquid layer and droplets on a vibrating flexible plate. Microgravity Sci. Technol. **30**, 1–2 (2018)

19. D. Sun, K.F. Böhringer, M. Sorensen, E. Nilsson, J.S. Edgar, D.R. Goodlett, Droplet delivery and nebulization system using surface acoustic wave for mass spectrometry. Lab Chip **20**, 17 (2020)

20. M. Roudini, D. Niedermeier, F. Stratmann, A. Winkler, Droplet generation in standing-surface-acoustic-wave nebulization at controlled air humidity. Phy. Rev. Appl. **14**, 1 (2020)

21. M.H. Biroun, M. Rahmati, M. Jangi, B. Chen, Y.Q. Fu, Numerical and experimental investigations of interdigital transducer configurations for efficient droplet streaming and jetting induced by surface acoustic waves. Int. J. Multiph. Flow **136**, 103545 (2021)

22. Z. Insepov, Z. Ramazanova, N. Zhakiyev, K. Tynyshtykbayev, Water droplet motion under the influence of Surface Acoustic Waves (SAW). J. Phy. Commun. **5**, 3 (2021)

23. W. Connacher, J. Orosco, J. Friend, Droplet ejection at controlled angles via acoustofluidic jetting. PRL **125**, 18 (2020)

24. J. Li, M.H. Biroun, R. Tao, Y. Wang, H. Torun, N. Xu, M. Rahmati, Y. Li, D. Gibson, C. Fu, J. Luo, Wide range of droplet jetting angles by thin-film based surface acoustic waves. J. Phys. D Appl. Phys. **53**, 35 (2020)

25. P. Brunet, M. Baudoin, Unstationary dynamics of drops subjected to MHz-surface acoustic waves modulated at low frequency. Exp. Fluids **63**, 1 (2022)

26. M.B. Özer, B. Çetin, An extended view for acoustofluidic particle manipulation: scenarios for actuation modes and device resonance phenomenon for bulk-acoustic-wave devices. JASA **149**, 4 (2021)

27. Y. Zhang, X. Chen, Particle separation in microfluidics using different modal ultrasonic standing waves. Ultrason. Sonochem. **75**, 105603 (2021)

28. A.G. Guex, N. Di Marzio, D. Eglin, M. Alini, T. Serra, The waves that make the pattern: a review on acoustic manipulation in biomedical research. Mater. Today Bio **10**, 100110 (2021)

29. Z. Liu, A. Fornell, M. Tenje, A droplet acoustofluidic platform for time-controlled microbead-based reactions. Biomicrofluidics **15**, 3 (2021)

30. M.H. Biroun, J. Li, R. Tao, M. Rahmati, G. McHale, L. Dong, M. Jangi, H. Torun, Y. Fu, Acoustic waves for active reduction of contact time in droplet impact. Phy. Rev. Appl. **14**, 2 (2020)

31. N. Zhang, A. Horesh, J. Friend, Manipulation and mixing of 200 femtoliter droplets in nanofluidic channels using MHz-order surface acoustic waves. Adv. Sci. **8**, 13 (2021)

32. Y. Wang, Q. Zhang, R. Tao, D. Chen, J. Xie, H. Torun, LE. Dodd, J. Luo, C. Fu, J. Vernon, P. Canyelles-Pericas, A rapid and controllable acoustothermal microheater using thin film surface acoustic waves, Sens. Actuators A: Phys., 318 (2021)

33. Y. Lei, H. Hu, J. Chen, P. Zhang, Microfluidic jetting deformation and pinching-off mechanism in capillary tubes by using traveling surface acoustic waves. Actuators **9**, 1 (2020)

34. D. Mandal, S. Banerjee, Surface acoustic wave (SAW) sensors: physics. Mater. Appl. Sens. **22**, 3 (2022)

35. A. Palla-Papavlu, S.I. Voicu, M. Dinescu, Sensitive materials and coating technologies for surface acoustic wave sensors. Chemosensors **9**, 5 (2021)

36. Q.Y. Huang, Q. Sun, H. Hu, J.L. Han, Y.L. Lei, Thermal effect in the process of surface acoustic wave atomization. Exp. Therm. Fluid Sci. **120**, 110257 (2021)

37. G. Lajoinie, T. Segers, M. Versluis, High-frequency acoustic droplet vaporization is initiated by resonance. PRL **126**, 3 (2021)

38. Y. Terakawa, J. Kondoh, Numerical and experimental study of acoustic wave propagation in glass plate/water/128YX-LiNbO$_3$ structure. JJAP **59**, SKKC08 (2020)

39. Q.Y. Huang, H. Hu, Y.L. Lei, J.L. Han, P. Zhang, J. Dong, Simulation and experimental investigation of surface acoustic wave streaming velocity. JJAP **59**, 6 (2020)

40. S.M. Sheikholeslam Noori, M. Taeibi, S.A. Shams Taleghani, Multiple relaxation time color gradient lattice Boltzmann model for simulating contact angle in two-phase flows with high density ratio. EPJP **134**, 8 (2019)

41. S.M. Sheikholeslam Noori, M. Taeibi, S.A. Shams Taleghani, Numerical analysis of droplet motion over a flat plate due to surface acoustic waves. Microgravity Sci. Technol. **32**, 4 (2020)

42. S.M. Sheikholeslam Noori, M. Taeibi, S.A. Shams Taleghani, Effects of contact angle hysteresis on drop manipulation using surface acoustic waves. Theor. Comput. Fluid Dyn. **34**, 1 (2020)

43. S.M. Sheikholeslam Noori, S.A. Shams Taleghani, M. Taeibi, Surface acoustic waves as control actuator for drop removal from solid surface. Fluid Dyn. Res. **53**, 4 (2021)

44. H. Ding, P.D. Spelt, Wetting condition in diffuse interface simulations of contact line motion. Phys. Rev. E **75**, 4 (2007)

45. P. Brunet, M. Baudoin, O.B. Matar, F. Zoueshtiagh, Droplet displacements and oscillations induced by ultrasonic surface acoustic waves: a quantitative study. Phys. Rev. E **81**, 3 (2010)

46. H.W. Zheng, C. Shu, Y.T. Chew, A lattice Boltzmann model for multiphase flows with large density ratio. J. Comput. Phys. **218**, 1 (2006)

47. T. Reis, T.N. Phillips, Lattice Boltzmann model for simulating immiscible two-phase flows. J. Phys. A Math. Theor. **40**, 14 (2007)

48. K. Hejranfar, E. Ezzatneshan, Simulation of two-phase liquid-vapor flows using a high-order compact finite-difference lattice Boltzmann method. Phys. Rev. E **92**, 5 (2015)

49. Y. Wang, X. Tao, R. Tao, J. Zhou, Q. Zhang, D. Chen, H. Jin, S. Dong, J. Xie, Y.Q. Fu, Acoustofluidics along inclined surfaces based on AlN/Si Rayleigh surface acoustic waves. Sens. Actuators A Phys. **306**, 111967 (2020)

50. S.M. Sheikholeslam Noori, S.A. Shams Taleghani, M. Taeibi, Phenomenological investigation of drop manipulation using surface acoustic waves. Microgravity Sci. Technol. **32**, 6 (2020)

51. J.D. Peterson, I. Bagkeris, V. Michael, A new framework for numerical modeling of population balance equations: solving for the inverse cumulative distribution function. Chem. Eng. Sci. **259**, 117781 (2022)

52. F. Cui, X. Geng, B. Robinson, T. King, K. Lee, M.C. Boufadel, Oil droplet dispersion under a deep-water plunging breaker: experimental measurement and numerical modeling. J. Mar. Sci. Eng. **8**, 4 (2020)

53. T. Matsoukas, Thermodynamics beyond molecules: statistical thermodynamics of probability distributions. Entropy **21**, 9 (2019)

54. W.G. Madden, E.D. Glandt, Distribution functions for fluids in random media. J. Stat. Phys. **51**, 3 (1988)

55. B. Widom, *Statistical Mechanics: A Concise Introduction for Chemists* (Cambridge University Press, 2004)

56. D. Williams, *Probability with Martingales* (Cambridge University Press, 1991)

57. R. Faillettaz, C.B. Paris, A.C. Vaz, N. Perlin, Z.M. Aman, M. Schlüter, S.A. Murawski, The choice of droplet size probability distribution function for oil spill modeling is not trivial. Mar. Pollut. Bull. **163**, 111920 (2021)
58. M.T. Rahni, S.A. Taleghani, M. Sheikholeslam, G. Ahmadi, Computational simulation of water removal from a flat plate, using surface acoustic waves. Wave Motion **111**, 102867 (2022)